Mechanics & Industry **19**, 305 (2018)
© AFM, EDP Sciences 2018
https://doi.org/10.1051/meca/2018011

Mechanics & Industry

Available online at:
www.mechanics-industry.org

Regular Article

A micromechanical scratch model to investigate wear mechanisms in UD-GFRP composites

Slah Mzali[1,*], Fatma Elwasli[1], Ali Mkaddem[2], and Salah Mezlini[1]

[1] Laboratoire Génie Mécanique, École Nationale d'Ingénieurs de Monastir, Université de Monastir Monastir, Tunisia
[2] Mechanical Engineering Department, Faculty of Engineering, University of Jeddah, PO. Box 80327, 21589 Jeddah, Saudi Arabia

Received: 29 June 2016 / Accepted: 10 February 2018

Abstract. This study suggests a micromechanical approach to scrutinize the glass fiber reinforced polyester (GFRP) composite tribological behavior. A single indenter scratch test (SST) using spherical tip conical indenter was adopted. The 3D finite element (FE) model was developed into ABAQUS/Explicit commercial code. Both material behavior and damage of polyester matrix and glass fiber was modeled using the Johnson Cook behavior law. Nevertheless, the fiber/matrix interface behavior is described using the cohesive zone approach via the cohesive elements. The elementary wear mechanisms owing to the SST were appraised at different attack angle and normal load by the mean of scanning electron microscope (SEM). In this work, the material removal map was built to emphasize the correlation between the tribological parameters, particularly the attack angle and the normal load, and the material removal process. The numerical results emphasized the significant effects of the attack angle and the penetration depth on the transition of the wear mechanisms from ploughing to composite damage. The experimental wear mechanisms and the predicted elementary wear mechanisms seem to be in a good agreement.

Keywords: Scratch / UD-GFRP / wear / friction / wear map / FE

1 Introduction

The surface integrity characterization can nowadays be considered as a big challenge in the development of several industries including transport, astronautics and aeronautics. The study of the surface integrity, particularly of the composite material requires in-depth knowledge of the abrasion tests which spotlight the local surface properties and contact behavior, including friction, adhesion and damage. The most used technique in characterization of both homogeneous [1] and heterogeneous [2,3] materials friction behavior is the scratch test.

Using the block on ring configuration Kim et al. [4] investigated the rubbing and the damage of short glass fibers reinforced polyamide composite. They studied the composite tribological behavior according to fibers' direction and rate and proved that the effect of fibers amount is significant on the composite wear rate which inversely evolve. They found that a weight glass fiber percent of 30 (wt%) gives a better composite wear resistance. They also demonstrated that the composite friction and damage were increasingly dependent on the fibers amount and the temperature.

Quintelier et al. [5] investigated the tribological behavior of the glass fiber reinforced polyester (GFRP) composites, utilizing pin-on-disk tribotester. They showed that the initial fibers fracture is mostly localized in a cross section irrespective of the fibers' orientation. When sliding perpendicularly to fiber orientation, the fibers are bending provoking longitudinal strains and generating initial fracture. However, sliding parallel to the fibers' orientation generates shearing forces due to high stresses. Based on SEM micrographs, they observed numerous elementary composite damage modes, particularly fiber fracture, interface debonding, matrix breakage and fiber pull out.

Though the experiments achieved good conclusions on homogeneous metallic or polymeric material behavior, they were incomplete and insufficient to provide a better comprehension of the composite materials behavior due to the complexities of the local mechanisms dominating. Therefore, with the aim of supporting the experimental investigations, the finite element (FE) analysis can hence be used. In recent years, several models for investigating the tribological behavior of homogeneous materials [6,7] have

* e-mail: mzalislah@hotmail.com

been developed. The FE analysis of composite materials is still, however, challenging and understudied.

For over a decade, Goda et al. [8] conducted an FE analysis of a composite material subjected to a sliding steel asperity. The sliding was performed normal to the fibers' orientation. They demonstrate that the suggested micro/macro FE approach adopted is more appropriate to predict the wear modes than the equivalent macro-mechanical approaches [9]. They studied the composite damage modes and showed that the high shear stress was in the origin of the matrix breaking with the appearance of thin films of wear debris. Nevertheless, high normal stresses, in the region of contact, provoke the crack of the backward fibers' edges. Besides, the experimentally-observed wear mechanisms, particularly fibers' cracking, interface debonding and matrix shear failure, were successfully emphasized.

Similar FE approach was adopted by Friedrich et al. [10]. They implemented a micromechanical model simulating the scratch of GFRP composite. The dominant wear mechanisms, when sliding parallel to the fibers' orientation, were highlighted, namely the fiber thinning, the fiber/matrix interface debonding and the shearing of the matrix. However, the sliding normal to the fibers' orientation appended the dominance of fibers' cracking wear mechanism. When confronting the predicted results to the experimental wear mechanisms, they proved the validity of their model.

This paper aims to implement micromechanical FE model to simulate different damage modes in UD-GFRP composite subjected to a sliding conical steel indenter. A special attention is devoted to the attack angle and the normal load effects. The FE micromechanical model suggested in this investigation was reliable enough to predict the local elementary damage modes versus the tribological parameters for the scratch test.

2 Materials and methods

2.1 Materials

The material used in this study is unidirectional glass fiber reinforced polyester (UD-GFRP) composite. Samples of $50 \times 50 \times 6.10^{-9}\,m^3$ were already prepared from pultruded rectangular section bar. The reinforcement material chosen is E glass long fiber with an average diameter of $23.10^{-6}\,m$ and a weight percentage of 21 (wt%). This UD-GFRP composite is filled with 14 wt% ASP400 clay filler. The scratches were performed on $50 \times 50.10^{-6}\,m^2$ facet.

2.2 Scratch test

SST was firstly carried out using a testing device as described by Mzali et al. [11]. In this investigation, the velocity and scratch length are both fixed at $210.10^{-3}\,m/min$ and $20.10^{-3}\,m$, respectively. Nevertheless, the normal load is ranging from 10 to 50 N by using dead weights. Indeed, this range covers the suitable normal load allowing us to sweep all possible wear scenarios: (i) indenter affects only the matrix and does not reach subsurface fiber layers, (ii) indenter damages the first fiber layer, (iii) indenter solicits a few fiber layers and (iv) indenter reaches many fiber layers. Furthermore, due to the different geometries of the abrasive grains, the attack angle is varying from 10° to 60°. A conical high speed steel indenter was used. All though the investigation tests were carried out without lubricant and each test was repeated three times using the same conditions. The different wear mechanisms were assessed through SEM. As defined by Coulomb's law, the apparent friction coefficient (μ_{app}) was computed by dividing the tangential load by the normal force.

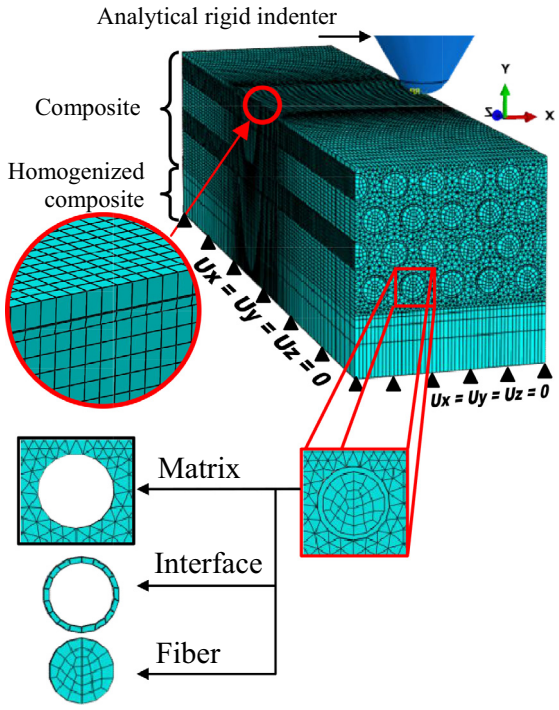

Fig. 1. SST mesh construction and boundary conditions.

2.3 FE micromechanical modeling

The FE code ABAQUS/Explicit was used to create and solve the FE micromechanical model. With the aim of avoiding convergence difficulties of the solution, the dynamic/explicit integration scheme was purposely adopted. When implementing the GFRP composite micromechanical models, numerous hypotheses concerning the constituents of the material, particularly the glass fiber reinforcement, the polyester matrix and the fiber/matrix interface, were proposed. The hexagonal regular fiber arrangement was chosen and a 21 wt% of fiber was selected.

2.3.1 Mesh and boundary conditions

With a view to simulating the SST using a spherical tip conical indenter, a 3D micromechanical model was implemented in the commercial FE software ABAQUS. In order to reduce the CPU time for this model, we just simulated the interest zone of the specimen. Hence, the sample, that has dimension of $187 \times 200 \times 800.10^{-18}\,m^3$, was divided into two rectangular parallelepiped parts. The bottom part is the homogenized composite. Nevertheless, the upper part is the composite with its three components: the fibers, the matrix, and the interfaces. Thereby, a total of 20 fibers and 20 interfaces were used in order to build the

composite section. Figure 1 shows the geometry, the mesh constructions and the boundary conditions adopted in the SST model. Once the convergence test was carried out, a mesh with 403 128 nodes and 316 215 elements was defined. The mesh discretization was purposely refined close to the contact zone between the indenter and the composite and elements of 3.75×10^{-6} m were used.

The interactions between the indenter and both fiber and matrix were controlled by the contact pairs' algorithm (surface to surface contact with slave surface type: node region). However, general contact algorithm defined the interactions at fiber/matrix and fiber/fiber interfaces. All interactions are controlled by the Coulomb friction model with an interfacial friction coefficient of about 0.13.

In this model, two steps were used to simulate the SST. Firstly, a vertical displacement of the indenter up to the target penetration was applied against the sample. Secondly, the scratching began with the indenter tangential sliding until the target scratch length (160.10^{-6} m). The bottom face of the sample was constrained while symmetry conditions were applied to its both right and left sides.

2.3.2 Material and failure modeling

With the aim of achieving a balance between efficiency and accuracy of the numerical computation results tow approach was used to analyze the UD-GFRP composite scratch behavior. The micromechanical approach describes the composite section which is modeled as multiphase's material (MPHM) constituted of glass fiber, polyester and interface phases. However, the homogeneous approach describes the homogenized composite which was modeled as an equivalent orthotropic homogeneous material (EOHM).

2.3.2.1 MPHM model

The matrix and the fiber were assimilated to be homogeneous isotropic elastoplastic material. Particularly, the behavior of the glass fiber was defined via standard tensile test conducted by Kim et al. [12]. The stress–strain curve obtained displayed a narrow transition region supposed to be typically plastic region. Therefore, Johnson–Cook constitutive criteria [13] were selected for modeling both behavior and damage of matrix and fibers. Furthermore, Johnson–Cook failure model was adopted owing to its capacity to take into consideration, in the same expression, the plastic strain, the strain rate and the failure. Its expression of the equivalent plastic flow stress is given by:

$$\sigma = \left(A + B\overline{\varepsilon^{\mathrm{pl}n}}\right)\left[1 + C\ln\left(\frac{\overline{\varepsilon}^{\mathrm{pl}}}{\overline{\varepsilon}_0}\right)\right]\left[1 - \left(\frac{T - T_{\mathrm{ref}}}{T_{\mathrm{melt}} - T_{\mathrm{ref}}}\right)^m\right], \tag{1}$$

where σ is the equivalent stress, $\overline{\varepsilon}^{\mathrm{pl}}$ is the equivalent plastic strain, $\overline{\varepsilon}^{\mathrm{pl}}$ and $\overline{\varepsilon}$ are the equivalent plastic and the reference strain rate, respectively. A is the initial yield stress, B is the hardening modulus, C is the strain rate dependency coefficient, n is the strain-hardening exponent, m is the thermal softening coefficient, T, T_{melt} and T_{ref} are the process, the melting and the bulk temperature, respectively.

Table 1. Composite constituents properties.

Material properties	Matrix [15]	Fiber [12]
E (GPa)	7	54
υ	0.4	0.21
ρ	1200	2550
Johnson-Cook behavior parameters		
A (MPa)	49	1340
B (MPa)	111	15 190
n	0.51	0.99
Johnson-Cook damage parameters		
$d1$	10^{-4}	10^{-7}
G_f (J/m^2)	100 [16]	500

The cumulative damage initiation model is defined by:

$$\omega = \sum \frac{\Delta\overline{\varepsilon}^{\mathrm{pl}}}{\overline{\varepsilon}_f^{\mathrm{pl}}} \tag{2}$$

where $\Delta\overline{\varepsilon}^{\mathrm{pl}}$ is the increment of equivalent plastic strain. $\overline{\varepsilon}_f^{\mathrm{pl}}$ is the equivalent strain at failure relaying between stress triaxiality, strain rate and temperature. It is given by:

$$\overline{\varepsilon}_f^{\mathrm{pl}} = \left[d_1 + d_2\exp\left(d_3\frac{p}{\sigma}\right)\right]\left[1 + d_4\ln\left(\frac{\dot{\overline{\varepsilon}}^{\mathrm{pl}}}{\dot{\varepsilon}_0}\right)\right]\left[1 + d_5\left(\frac{T - T_{\mathrm{ref}}}{T_{\mathrm{fus}} - T_{\mathrm{ref}}}\right)\right], \tag{3}$$

where $d_{i,i=1\ldots5}$ are the failure parameters.

The damage evolution (D). was expressed as the ratio between the equivalent plastic displacement ($\overline{u}^{\mathrm{pl}}$) and the displacement at failure ($\overline{u}_f$pl). D ranges from 0 to 1 and can be defined as a linear function of equivalent plastic strain. It expressed as:

$$D = \frac{\overline{u}^{\mathrm{pl}}}{\overline{u}_f^{\mathrm{pl}}} = \frac{L_{\min}\overline{\varepsilon}^{\mathrm{pl}}}{\overline{u}_f^{\mathrm{pl}}} = \frac{2G_f L_{\min}\overline{\varepsilon}^{\mathrm{pl}}}{\sigma_{y0}}, \tag{4}$$

where $L_{\min}$ is the minimal characteristic length of the FE mesh. σ_{y0} Is the flow stress at damage initiation. G_f is the material failure energy expressed as follows:

$$G_f = \int_{\overline{\varepsilon}_0^{\mathrm{pl}}}^{\overline{\varepsilon}_f^{\mathrm{pl}}} L_{\min}\sigma_y d\overline{\varepsilon}^{\mathrm{pl}} = \int_{\overline{u}_0^{\mathrm{pl}}}^{\overline{u}_f^{\mathrm{pl}}} \sigma_y d\overline{u}^{\mathrm{pl}}. \tag{5}$$

The matrix and the fibers properties and damage parameters used in the proposed model are summarized in Table 1. In this study, we neglected the dependence of damage on triaxiality ($d_2 = d_3 = 0$), strain rate ($d_4 = 0$) and temperature ($d_5 = 0$). Thus, there is one remaining

parameter d_1 describing the equivalent plastic strain size at the failure beginning. Similar hypothesis were adopted by Tenorio and Pelegri [14]. The Johnson–Cook parameters were computed using inverse approach [15,16] upon a Matlab routine.

The glasser/polyester interface was discretized using finite cohesive elements. The traction separation law implemented under ABAQUS/Explicit (type: QUADS) was adopted to simulate the interface failure. The cohesive constitutiveolves lr elastic behavior associated with damage concepts, namely, initiation and evolution. The elastic-linear softening constitutive model can be written as:

$$\begin{Bmatrix} t_n \\ t_s \\ t_t \end{Bmatrix} = \begin{bmatrix} K_{\mathrm{nn}} & K_{\mathrm{ns}} & K_{\mathrm{nt}} \\ K_{\mathrm{ns}} & K_{\mathrm{ss}} & K_{\mathrm{st}} \\ K_{\mathrm{nt}} & K_{\mathrm{st}} & K_{\mathrm{tt}} \end{bmatrix} \begin{Bmatrix} \varepsilon_n \\ \varepsilon_s \\ \varepsilon_t \end{Bmatrix}, \tag{6}$$

where t is the nominal traction stress vector which has three components: t_n, t_s and t_t representing the normal and tow shear traction, respectively. Kij is the stiffness coefficient. ε_n is the nominal strain and ε_s, ε_t are the shear strains.

The damage initiation is simulated using the quadratic nominal stress criterion. Damage initiate, when, this criterion involving the nominal stress ratios reaches a unit. This criterion is written as:

$$\left(\frac{t_n}{t_n^0}\right)^2 + \left(\frac{t_s}{t_s^0}\right)^2 + \left(\frac{t_t}{t_t^0}\right)^2 = 1, \tag{7}$$

with t_n^0,t_s^0, t_t^0 refer to the maximum stresses. The angle brackets $\langle\rangle$ designates that the pure compression causes no damage initiation. When damage initiation is achieved the cohesive strength degradation starts.

The damage evolution provoked by the growth of delamination utilizes a mixed-mode fracture energy criterion given by Benzeggagh and Kenane [17–21]. The fracture is supposed consisting of three modes. The first one is provoked by the interlaminar tension (an opening Mode I, G_{I}). The interlaminar shear promotes the sliding shear Mode II (G_{II}) and anti-plane shear induces the scissoring shear Mode III (G_{III}). Delamination is supposed to initiate once the energy release rate (G) reaches the material fracture toughness ($G = G_c$). Thus, the three-dimensional failure criterion can be written as:

$$G = G_{\mathrm{Ic}} + (G_{\mathrm{IIc}} - G_{\mathrm{Ic}}) \left\{\frac{G_{\mathrm{shear}}}{G_T}\right\}^{\eta}, \tag{8}$$

where G_{Ic} and G_{IIc} are the fracture toughness of pure mode. $G_{\mathrm{shear}} = G_{II} + G_{III}$ is the energy release rate under shear loading. $G_T = G_{\mathrm{I}} + G_{\mathrm{shear}}$ is the energy release rate for mixed-mode loading [18,19]. The interface properties are summarized in Table 2.

2.3.2.2 EHOM model

The equivalent homogeneous orthotropic material (EHOM) assumptions were used to model the homogenized composite. Based on the approach proposed by Chamis [22], the elastic constants were determined (Tab. 3).

Table 2. Interface behavior properties.

Traction-separation law (QUADS) [16]	
Damage initiation	
(MPa)t_n^0	50
t_s^0 (MPa)	75
t_t^0 (MPa)	75
Damage evolution	
(J/m^2) G_n^C	10
G_s^C (J/m^2)	25
G_t^C (J/m^2)	25

Table 3. EHOM mechanical properties.

Mechanical properties	
E_1 (GPa)	22.98
E_2 (GPa)	14.21
E_3 (GPa)	14.21
υ_{12}	0.33
υ_{13}	0.33
υ_{23}	0.37
G_{12} (GPa)	5.18
G_{13} (GPa)	5.18
G_{23} (GPa)	5.18

$$E_1 = V^f E^f + V^m E^m, \tag{9}$$

$$E_2 = E_3 = \frac{E^m}{1 - \sqrt{V^f}\left(1 - \frac{E^m}{E^f}\right)}, \tag{10}$$

$$\vartheta_{12} = \vartheta_{13} = V^f \vartheta^f + V^m \vartheta^m, \tag{11}$$

$$\vartheta_{23} = \frac{E_2}{2G_{23}} - 1, \tag{12}$$

$$G_{12} = G_{13} = G_{23} = \frac{G^m}{1 - \sqrt{V^f}\left(1 - \frac{G^m}{G^f}\right)}. \tag{13}$$

With E_i, υ_{ij} and G_{ij} are the Young's modulus, the Poisson's ratios and the shear modulus of the homogenized composite in i and j directions, respectively; E^m and E^f are the matrix and fibers Young's modulus, respectively; υ^m and υ^f are the matrix and fibers Poisson's ratios, respectively; and V^m and V^f are the matrix and fibers' volume fraction, respectively.

3 Results and discussion

3.1 SST wear mechanisms

To emphasize the SST wear mechanisms, SEM micrographs observations were carried out. With a view to having a better comprehension of the GFRP composite

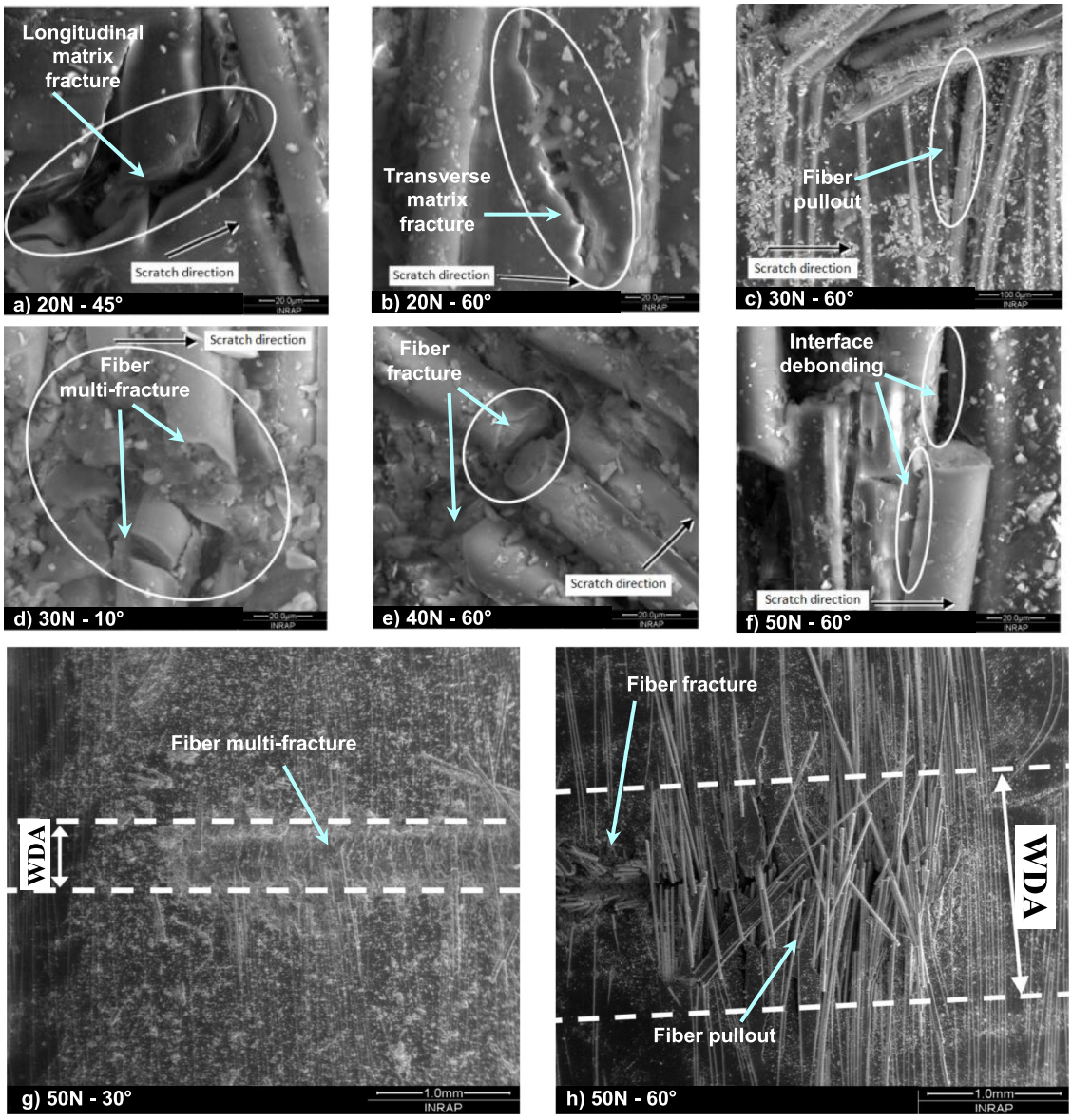

Fig. 2. Typical SEM micrographs emphasizing the damage mechanisms under SST. (a, b) $F_n = 20\,\text{N}$, (c, d) $F_n = 30\,\text{N}$, (e) $F_n = 20\,\text{N}$ and (f–h) $F_n = 50\,\text{N}$.

behavior, microscopic investigation was conducted. Figure 2 shows several wear mechanisms generated by SST. Different damage mechanisms were perceived, namely the matrix transverse and longitudinal fracture, the debonding of the interface between fiber and matrix, the fibers fracture, multi-fractures and pull out. The coexistence of several damage mechanisms is prospective in the same groove. Whereas, the prevailing wear mechanism depends on the applied tribological parameters.

The SST allowed us to identify the wear mechanisms of composite material. Unlike homogeneous materials, where the damaged area is generally around the groove generated by the indenter, the damaged area of composite material can be spread over a wider area. More specifically, the phenomenon of fiber pullout can greatly enlarge the damaged area.

Figures 2g, 2h displays a comparison between two damage modes. It shows that the width of the damaged area (WDA) depends on the wear mechanisms. Indeed, for a low attack angle, fibers multi-fractures are essentially observed in the contact area. The indenter generates a groove with almost constant width.

The WDA is about $568.10^{-6}\,\text{m}$ (Fig. 2g). However, large attack angle increases the contact radius between the indenter and the surface layers of fibers. The debonding of the fiber/matrix interface privileges traction of the fibers, which are generally fractured in sections far away from the scratch direction. Therefore, the phenomenon of fiber pullout will be prevailing. Thus, the spread WDA is tripling to reach $1730.10^{-6}\,\text{m}$ (Fig. 2h).

The evolution of the approximate WDA versus test parameters, including the attack angle and the normal load, is plotted in Figure 3. Low attack angle ($\theta \leq 30°$)

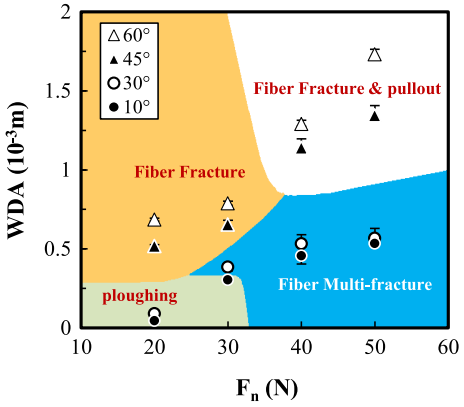

Fig. 3. Wear map (WDA vs. F_n and θ).

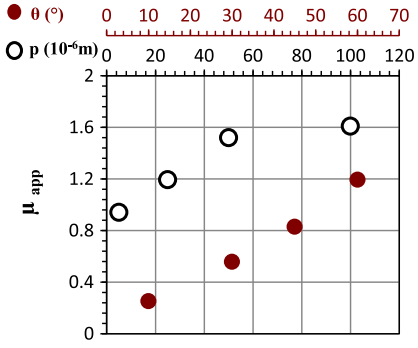

Fig. 4. Predicted apparent friction coefficient vs. penetration p ($\theta = 60°$), and attack angle θ ($p = 25.10^{-6}$ m).

generates dominant wear modes such as ploughing and fiber multi-fractures. Indeed, WDA remains below 600.10^{-6} m, and the ploughing domain presents the lowest WDA. However, the transition of prevailing wear mechanisms to fibers fracture, for low normal load 20 and 30 N, and fibers fracture/pullout, for large normal load 40 and 50 N, in the case of high attack angles ($\theta \geq 45°$) increases the WDA. The maximum value is obtained for the most severe conditions ($F_n = 50$ N, $\theta = 60°$) and reaches 1730.10^{-6} m.

3.2 Sensitivity of friction to penetration and attack angle

With a view to studying the influence of the penetration depth, SST simulations with conical indenter of 60° attack angle and several penetrations ranging from 5.10^{-6} to 100.10^{-6} m were conducted. These penetrations were selected in order to sweeping all probable configurations. Low penetration depth of 5.10^{-6} m allows the indenter to penetrate only on the matrix. The first fibers layer is not affected. When the penetration of the indenter is about 25.10^{-6} m, the first fiber layer is barely reached. Only the first fibers layer is affected, when penetration is about 50.10^{-6} m. Nevertheless, 100.10^{-6} m penetration depth allows the indenter to scratch several fibers layers.

In order to study the influence of the attack angle, the same experimental attack angles (10, 30, 45 and 60°) were used in the simulations of the SST. A constant penetration depth of 25.10^{-6} m is selected. With the view to promoting the indenter conical part effect, a tip radius of 10.10^{-6} m is used.

Figure 4 shows predicted apparent friction coefficient evolution as function of penetration and attack angle. It proves that predicted apparent friction coefficient is very sensitive to penetration depth below 50 μm. In fact, increasing the penetration depth from 5.10^{-6} to 50.10^{-6} m, increases predicted apparent friction coefficient by about 60%. However, an increase of just 6% is marked when penetration increases from 50.10^{-6} to 100.10^{-6} m. According to Figure 4, linear increase of predicted apparent friction coefficient with the attack angle is perceived. Hence, the predicted apparent friction coefficient is more sensitive to the conical indenter geometry. The same result was already proven experimentally by Mzali et al. [11]. When low attack angles were used, a large contact surface was observed, and the indenter rubs like a spherical pin. No material damage occurs. Under these conditions, low tangential load was generated to resist the indenter sliding. Therefore, low predicted apparent friction coefficient of 0.25 was perceived. Conversely, when large attack angles were used, lower contact surface was observed. Moreover, the penetration of the indenter against material and the scratching provokes greater resistance load. Consequently, the predicted apparent friction coefficient increases significantly and it is almost quintupled for the larger attack angle (60°).

3.3 Predicted elementary wear mechanisms vs. attack angle

The suggested model enables also to simulate the material damage mechanisms for a constant penetration of 25.10^{-6} m. Figure 5 shows the typical material removal mechanisms as a function of lower (10°) and larger (60°) attack angles. According to the numerical simulations results, the following remarks can hence be drawn.

θ=10°: the plastic flow of the material takes place. The matrix is essentially deformed plastically, but some matrix transverse fracture zones just above the surface layer of glass fibers appear. Indeed, experimental SST results showed similar material removal mechanisms (Fig. 5a). Nonetheless, the glass fibers were not affected and no fiber fracture happened (Fig. 5b). The prevailing wear mechanism was the debonding of the interface between fiber and matrix (Fig. 5c). This material removal process was propagated over a large region below the contact zone between the sample and the indenter. According to the experimental observation we cannot see this damage mechanism.

θ=60°: All the composite components were damaged. Wear modes like longitudinal matrix fracture (Fig. 5a), fiber damage (Fig. 5b) and fiber/matrix interface debonding (Fig. 5c) were perceived. The matrix fracture is basically shown in the contact area with the indenter. The first layer of fibers is scratched by the conical indenter tip which does not exceed the fiber diameter. Thus, the fibers' damage starts. Increasing the attack angle up to 60° provokes the damage mode transition from plastic ploughing to the longitudinal matrix fracture, the debonding of the fiber/matrix interface and the fiber damage. Similar damage modes were experimentally shown when scratching composite under similar conditions by Mzali et al. [11].

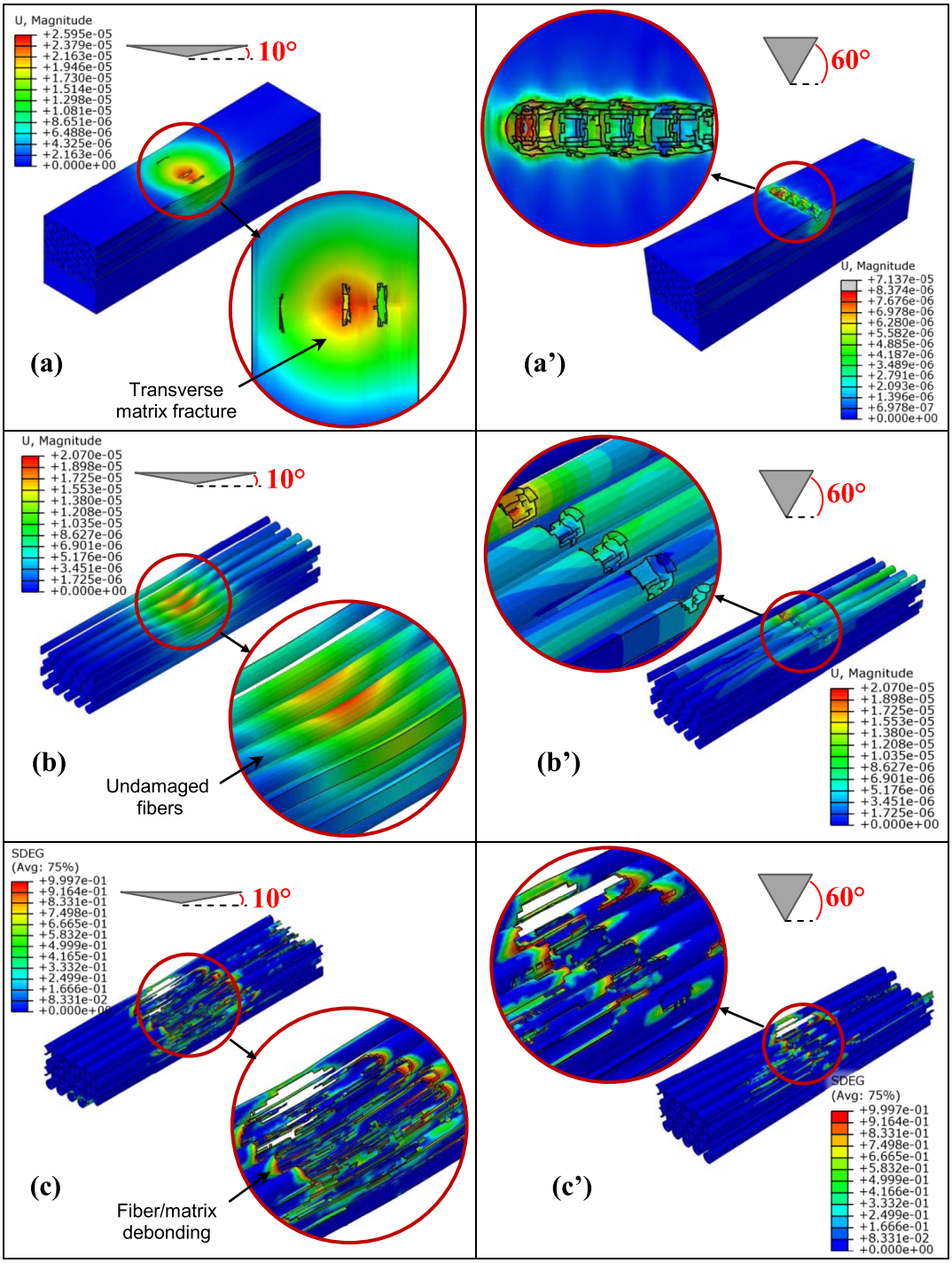

Fig. 5. Material removal process obtained by the proposed SST model for the extreme attack angles (10° and 60°) of (a) the matrix, (b) the fibers, and (c) the fiber/matrix interface.

3.4 Predicted elementary wear mechanisms vs. penetration depth

Figure 6 shows the composite material removal mechanisms for the two extreme depths of penetration 5.10^{-6} and 100.10^{-6} m and an angle attack of 60°. If the penetration of the indenter is very low, a scratch with a small width is obtained. In such case, the indenter begins to penetrate into the material damaging the polyester matrix (Fig. 6a). Figure 6b shows the equivalent plastic strain distribution in the fibers. A concentration of the fibers plastic deformation is observed at the contact with the indenter. This region becomes a probable zone of initiation of damage and fibers fracture. The fiber/matrix interface is slightly damaged (Fig. 6c). The damage is located just above the indenter at the interfacial layer.

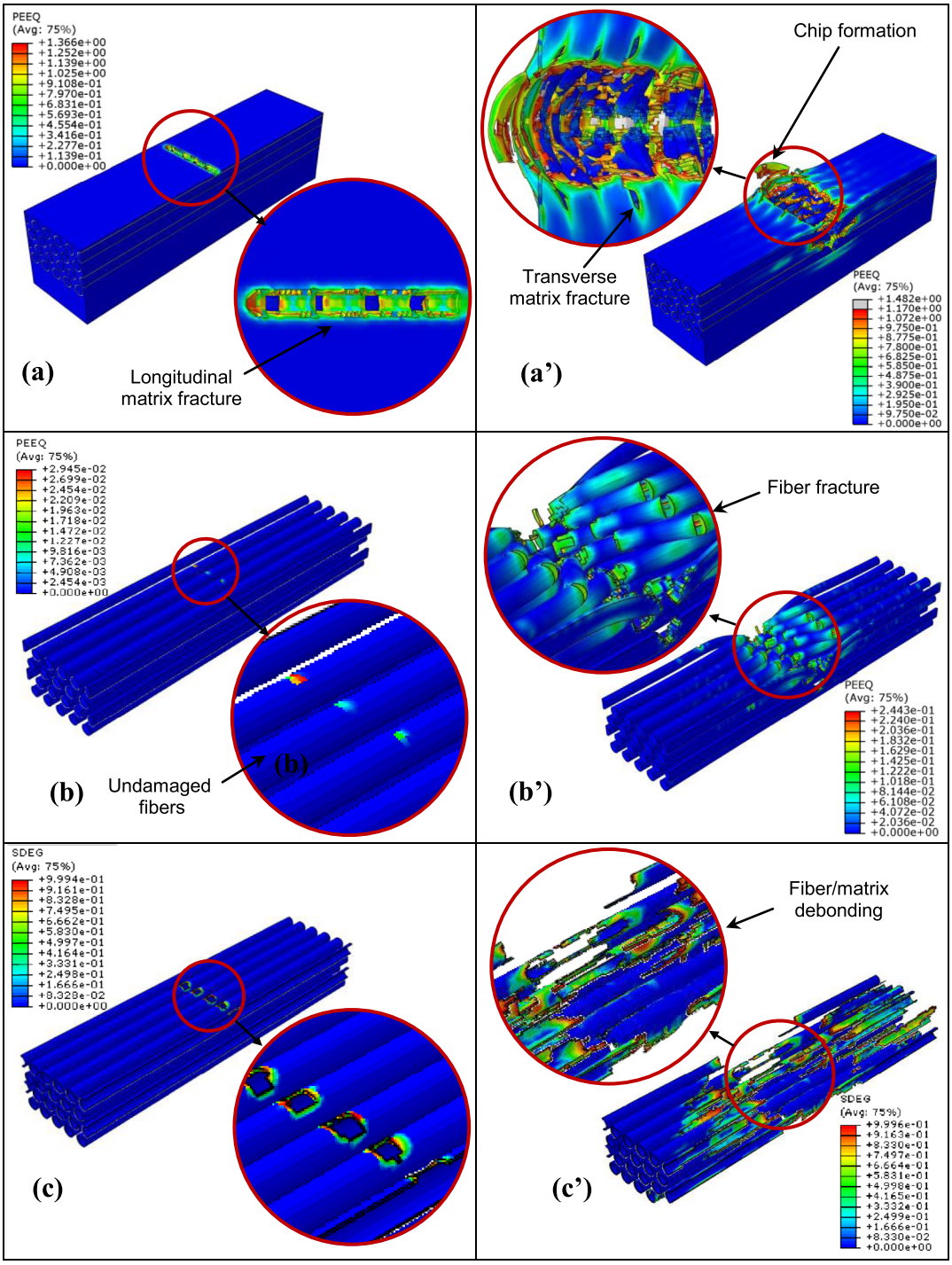

Fig. 6. Material removal process obtained by the proposed SST model for the extreme penetration (5.10^{-6} and 100.10^{-6} m) of (a) the matrix, (b) the fibers, and (c) the fiber/matrix interface.

However, a greater penetration depth generates a higher width. Under these conditions, the indenter penetrates into the composite by damaging both the matrix (Fig. 6a), the fibers (Fig. 6b) and the fiber/matrix interfaces (Fig. 6c). Two material removal process of the matrix are observed. The first one is the longitudinal breaking generated by the penetration and the sliding of the indenter. The formation of a frontal chip is perceived with the appearance of wear debris. The second one is the matrix transverse rupture induced by the fibers stretching after the fiber/matrix interface debonding. Transverse cracks appear in the matrix and increase the WDA which is 36% larger than the scratch width. Fibers' fracture is observed in two zones. The first region is located in the frontal contact with the indenter which deforms the fiber and stretches it until the occurrence of fracture with

debris of fractured fibers. The second region is located at both lateral sides of the scratch. The fibers stretched by the indenter causing transverse rupture of the matrix are then fractured. The debonding of the fiber/matrix interface is spread over a very large area marking the breakaway of the fiber from the matrix. This debonding can, thereafter, cause a probable occurrence of the fibers pull-out.

4 Conclusion

In this study, experimental and numerical investigation on scratch responses of UD-GFRP composite has been conducted. FE modeling was used to simulate SST of glass fiber/polyester composite. Particular attention was given to highlighting the effect of tribological parameters in the local material damage modes. The following conclusions can, therefore, be drawn.

- The local material removal process has been discerned through the SEM observation. Furthermore, the tribological parameters, particularly, the normal load and the attack angle govern the action limits of the dominant wear mechanisms in SST. Indeed, the increase of the attack angle provokes the switch of the dominant damage mode from ploughing to fiber fracture and fiber pullout. The Assessment of WDA reveals high sensibility of the damaged area to prevailing material removal process and testing parameters.
- The predicted apparent friction coefficient is fundamentally dominated by the tribological parameters. It increases when the penetration increases. Higher sensibility of the predicted apparent friction coefficient to the attack angle was proved. The larger the attack angle is, the higher the predicted apparent friction coefficient gets.
- The proposed FE analysis using the 3D SST micromechanical model has been found valuable to predict the local elementary damage mechanisms of UD-GFRP composite. A successful prediction of wear mechanisms versus the tribological parameters is carried out and found that the simulation results are in good agreement with the SEM observation.

References

[1] K. Elleuch, S. Mezlini, N. Guermazi, P. Kapsa, Abrasive wear of aluminium alloys rubbed against sand, Wear 261 (2006) 1316–1321

[2] S. Mezlini, M.B. Tkaya, M.E. Mansori, H. Zahouani, P. Kapsa, Correlation between tribological parameters and wear mechanisms of homogeneous and heterogeneous material, Tribol. Lett. 33 (2009) 153–159

[3] G. Gyawali, B. Joshi, K. Tripathi, S.W. Lee, Preparation of Ni-W-Si3N4 composite coatings and evaluation of their scratch resistance properties, Ceram. Int. 42 (2016) 3497–3503

[4] S.S. Kim, M.W. Shin, H. Jang, Tribological properties of short glass fiber reinforced polyamide 12 sliding on medium carbon steel, Wear 274 (2012) 34–42

[5] J. Quintelier, P.D. Baets, P. Samyn, D.V. Hemelrijck, On the SEM features of glass-polyester composite system subjected to dry sliding wear, Wear 261 (2006) 703–714

[6] F. Wredenberg, P.L. Larsson, Scratch testing of metals and polymers: experiments and numerics, Wear 266 (2009) 76–83

[7] A. Meneses-Amador, L.F. Jiménez-Tinoco, C.D. Reséndiz-Calderon, A. Mouftiez, G.A. Rodríguez-Castro, I. Campos-Silva, Numerical evaluation of scratch tests on boride layers, Surf. Coat. Technol. 284 (2015) 182–191

[8] T. Goda, K. Váradi, K. Friedrich, H. Giertzsch, Finite element analysis of a polymer composite subjected to a sliding steel asperity, J. Mater. Sci. 37 (2002) 1575–1583

[9] G. Perillo, F. Grytten, S. Sorbo, V. Delhaye, Numerical/experimental impact events on filament wound composite pressure vessel, Compos. Part B Eng. 69 (2015) 406–417

[10] K. Friedrich, K. Váradi, T. Goda, H. Giertzsch, Finite element analysis of a polymer composite subjected to a sliding steel asperity Part II: parallel and anti-parallel fibre orientations, J. Mater. Sci. 37 (2002) 3497–3507

[11] S. Mzali, S. Mezlini, M. Zidi, Effect of tribological parameters on scratch behaviour of unidirectional E-glass fibre reinforced polyester composite, Tribol. Mater. Surf. Interfaces 7 (2013) 175–182

[12] T. Kim, K. Oshima, H. Kawada, Impact tensile properties and strength development mechanism of glass for reinforcement fiber, International symposium on dynamic deformation and fracture of advanced materials D2FAM 2013, J. Phys. Conf. Ser. (2013) 012006

[13] G.R. Johnson, W.H. Cook, A constitutive model and data for metals subjected to large strains, high strain rates and high temperatures, 7th International Symposium on Ballistics, The Hague, The Netherlands, 1983, pp. 541–547

[14] M. Tenorio, A.A. Pelegri, Interfacial debonding of glass single fiber composites using the Johnson–Cook failure model, ASME 2013, in: International Mechanical Engineering Congress and Exposition, IMECE 2013, San Diego, CA, 2013, pp. 16–23

[15] A. Ershad-Langroudi, Etude de la déformation viscoélastique et plastique du PET amorphe et semi-cristallin autour de la transition vitreuse, Thèse, National Institute of Applied Sciences, Lyon, 1999

[16] D.A. Vajari, A micromechanical study of porous composites under longitudinal shear and transverse normal loading, Compos. Struct. 125 (2015) 266–276

[17] M.L. Benzeggagh, M. Kenane, Measurement of mixed-mode delamination fracture toughness of unidirectional glass/epoxy composites with mixedmode bending apparatus, Compos. Sci. Technol. 56 (1996) 439–449

[18] J. Li, J.K. Sen, Analysis of frame-to-skin joint pull-off tests and prediction of the delamination failure, in: Proceedings of 42nd AIAA/ASME/ASCE/AHS/ASC/Structures, Structural Dynamics, and Materials Conference, American Institute of Aeronautics and Astronotics, Seattle, USA, 2001, pp. 1–7

[19] J. Li, Three-dimensional effects in the prediction of flange delamination in composite skin-stringer pull-off specimens, J. Compos. Tech. Res. 24 (2002) 180–187

[20] A. Turon, P.P. Camanho, J. Costa, C.G. Davila, An interface damage model for the simulation of delamination under variable-mode ratio in composite materials, Nasa Center for AeroSpace Information NASA/TM-2004-213277, 2004, pp. 1–32

[21] D.S. Simulia, Abaqus 6.12, Analysis user's manual volume v: prescribed conditions, constraints & interactions, Abaqus Inc., 2012

[22] C.C. Chamis, Mechanics of composite materials: past, present, and future, J. Compos. Technol. Res. 11 (1989) 3–14

Cite this article as: S. Mzali, F. Elwasli, A. Mkaddem, S. Mezlini, A micromechanical scratch model to investigate wear mechanisms in UD-GFRP composites, Mechanics & Industry **19**, 305 (2018)